Measurement of mechanical properties for dense and porous polymer films having a low dielectric constant

Yuhuan Xu, Yipin Tsai, D. W. Zheng, K. N. Tu, Chung Wo Ong et al.

Citation: J. Appl. Phys. **88**, 5744 (2000); doi: 10.1063/1.1287756

View online: http://dx.doi.org/10.1063/1.1287756

View Table of Contents: http://jap.aip.org/resource/1/JAPIAU/v88/i10

Published by the American Institute of Physics.

Measurement of mechanical properties for dense and porous polymer films having a low dielectric constant

Yuhuan Xu, Yipin Tsai, D. W. Zheng, and K. N. Tu[a)]
Department of Materials Science and Engineering, UCLA, Los Angeles, California 90095-1595

Chung Wo Ong and Chung Loong Choy
Department of Applied Physics and Materials Research Center, Hong Kong Polytechnic University, Hong Kong

Bin Zhao, Q.-Z. Liu, and Maureen Brongo
Conexant Systems, Newport Beach, California 92660-3095

(Received 1 March 2000; accepted for publication 1 June 2000)

We measured the mechanical properties of dense and porous polymeric films, the modified polyarylethers, which have a low dielectric constant varying from 2.7 to 1.8, by combining three different methods; membrane bulge test, nanoindentation, and single-substrate bending beam method. The elastic modulus and initial stress measured from these three methods are in good agreement. The substrate effect was observed in the measurements by nanoindentation. Data obtained by nanoindentation show a significant dependence on the film thickness and the displacement depth of the indenter. However, the hardness of the low dielectric constant thin film does not depend on thickness and only slightly depends on the indentation depth. A tentative analysis is proposed to explain the results. © *2000 American Institute of Physics.* [S0021-8979(00)10217-8]

I. INTRODUCTION

Miniaturization has been the major reason of performance improvement of microelectronic devices. Faster device speed, higher device packing density, and more functions on a silicon chip have been achieved. For the ultra-large-scale-integration (ULSI) devices, while the transistor capacitance and resistance are reduced, the line-to-line capacitance and resistance of the metal interconnects are nevertheless increased. As a result, the resistance-capacitance (RC) delay of the metal interconnect will limit chip performance. Hence, there is an urgent need to reduce both the dielectric constant of interlayer dielectric materials (ILD) and the resistance of metal lines. It is known that the gain from a better dielectric material is greater than that from a better conductor. The substitution of SiO_2 ($\epsilon' = 4$) by air ($\epsilon' = 1$) will reduce the RC delay by a factor of 4, while the replacement of Al by Cu will only reduce the delay by approximately 35%.[1] Clearly, we must pursue the low ϵ' materials. According to the SIA (Semiconductor Industry Association) roadmap,[2] by the year 2001 the minimum feature size will be 0.18 μm, and the device will require an ILD with $\epsilon' = 2.3$. For later device generations, $\epsilon' < 2$ will be necessary.

Currently, research on low dielectric constant materials is intensive. Various low ϵ' materials are under investigation, including fluorinated silica glass,[3] amorphous C:F,[4] ''air gap'' formation,[5] nonfluorinated polymers,[6] poly (arylethers),[7] inorganic–organic hybrids,[8] porous polymers (e.g., methyl silsesquioxane[9]), and porous silica materials (''aerogel'' dried by supercritical methods or ''xerogel'' dried by solvent evaporation at ambient pressure).[10,11] Besides dielectric constant, other properties related to electrical, chemical, mechanical, thermal behaviors, and process compatibility and integration of these low dielectric constant materials are being studied.[12–14]

The polymeric poly(arylethers) (PAE) films have been used as the base material in our study. The PAEs are groups of aromatic polymers that can better withstand temperature cycling up to 450 °C than aliphatic polymers. The PAEs have dielectric constants between 2.6 and 2.9, glass transition temperatures T_g between 260 and 450 °C, moisture uptake lower than 1.5 wt. %, and gap filling capability in gaps less than 0.15 μm.[7] A series of modified poly(arylethers) (simply, also called PAE) films having low dielectric constants which can reach 1.8 was reported in one of our earlier papers.[15] Since the materials contain different amount of pores, their thermal and mechanical properties are of serious concern. The thermal conductivity for both dense and porous PAE polymeric films were measured.[16] Yet very little is known about the mechanical properties of these films, such as Young's modulus (E), Poisson's ratio (γ), residual stress, coefficient of thermal expansion (CTE), and hardness (H).

As far as metrology is concerned, for films with a thickness about 1 μm, a dual-substrate bending beam technique was developed for on-wafer measurements of elastic biaxial modulus and CTE.[17,18] Then the bulge test method can be used to measure the residual stress and biaxial modulus of metal, semiconductor, and some dielectric films with high resolution.[19,20] Nevertheless, it has rarely been applied to polymeric films except polyimide.[21,22] This is because of the difficulty in sample preparation of very thin and pinhole free

a)Electronic mail: kntu@ucla.edu

polymer membranes. The polyimide films tested in Refs. 21 and 22 are several microns in thickness. However, for the interlayer dielectric (ILD) materials used in CMOS, the film thickness is typically about a micron or less, therefore a reliable sample preparation technique for low ϵ' materials is needed. On the other hand, the nanoindentation method is one of the simplest ways to measure the Young's modulus and hardness of a thin film deposited on a substrate.[23,24]

In this article we report the combination of the membrane bulge test method, nanoindentation method, and single-substrate bending beam method to measure the mechanical properties and CTE for both dense and porous PAE films.

II. EXPERIMENT

A. Measurement of biaxial modulus by membrane bulge test

For preparing the membrane samples, dense and porous (porosity was evaluated to be 38%) PAE thin films were fabricated on silicon substrates[15] having square windows of area of $1.8\times1.8\,\mathrm{mm}^2$, which was prepared by generic lithography and Si backetching. The Si windows were etched using XeF_2 to form windows of PAE membranes of low ϵ'. The thickness of the membranes was measured by Tencor Alpha-Step 200. The details of sample processing have been described in Refs. 15 and 25.

The raw data of the bulge test provide the total deflection ''δ'' of the membrane under certain differential pressure ''P.'' For the square membrane test samples, there are two approaches to extract the initial stress and biaxial modulus from the raw data. The first is a direct fit between P and δ. The analytical formula given by Pan *et al.*[21] is

$$P=C_1 t\sigma_0\delta/a^2+C_2 f(\gamma)tE\delta^3/a^4(1-\gamma), \tag{1}$$

where $C_1=3.41$, $C_2=1.37$, $f(\gamma)=1.446-0.427\gamma$, a is half of the length of each side of the square, γ is the Poisson's ratio, σ_0 is the residual stress, t is the film thickness, and $E/(1-\gamma)$ is the biaxial modulus of the film. The second[26] is to calculate the stress σ and strain S at the center of the membrane:

$$\sigma=Pa^2/C_3 t\delta, \tag{2}$$

$$S=C_4\delta^2/a^2, \tag{3}$$

where $C_3=3.04$ and $C_4=0.451$ for square-shaped membranes. The Poisson's ratio γ was assumed to be 0.42 in the calculation (the choice of $\gamma=0.42$ will be explained in Sec. III.

B. Measurement of elastic modulus and hardness by nanoindentation

Nanoindentation measurements were performed using a Nanoindenter IIs (Nano Instruments, Inc.) to determine the elastic modulus (E) and hardness (H) of the dense and porous PAE films. The analysis method proposed by Oliver *et al.* was applied to manipulate the values of E and H.[27] In principle, the displacement (h) of a diamond tip and the normal load (P) applied are recorded continuously during indentation. The slope dP/dh of the unloading curve at $P_{\max}$ is defined to be the stiffness s. The displacement associated with the elastic deformation is $h_e=0.74\,P_{\max}/s$. The displacement related to the plastic deformation (contact depth) is $h_c=h_t-h_e$, where h_t is the overall displacement at $P_{\max}$. The area function of the diamond tip was carefully calibrated from which the contact area between the tip and the sample A at $h=h_c$ was determined. The value of E and H were obtained as

$$E=(\pi/A)^{1/2}(s/2), \tag{4}$$

and

$$H=P_{\max}/A. \tag{5}$$

Indentations were made on the surface of a film in a 6×6 matrice (36 points). The six indents in one row were produced by using the same experimental setting. Each indentation experiment consists of an approach segment, three load–hold–unload segments with successively increasing maximum loads, and finally a hold segment for correcting the thermal drift.

The maximum normal load was varied in the range of 3–700 μN. The corresponding indentation depth varied from about 10 to 300 nm. Since the sample was expected to be soft, in order to minimize the sinking of the diamond tip during the surface find process, different approaching speeds (1, 4, 5, and 10 nm sec^{-1}) and stiffness changes (2 and 4 times) for detecting sample surface were tried. In addition, different holding times (10 and 30 s) used in the hold segments before unloading were used to evaluate the influence of creep. It was found that the different setting did not produce any observable difference of results, such that an approaching rate of 4 nm sec^{-1} and a four-time stiffness change for surface detection were employed in all tests. A Poisson's ratio of 0.42 was used when calculating the values of E and H.

C. Measurement of CTE and initial stress by single-substrate bending beam method

In order to estimate the coefficient of thermal expansion of the dense and porous PAE film, the thermal stress was measured using a Flexus 2-300 machine (KLA-Tencor, CA) under a nitrogen flow of 3 l/min. The substrates used were 320 μm thick double-side-polished 4 in. silicon wafers. The PAE films were coated on one side of the wafer and the wafer curvature was measured from the other side. The dense and porous PAE films were coated at 3000 and 4000 rpm and then cured at 400 and 350 °C, respectively, for 30 min.[15] Four samples of each kind were tested. The initial stress and thermal stress can be obtained from Stoney's equation

$$\sigma_f=(E/1-\gamma)_s t_s^2/6t_f R, \tag{6}$$

where E is the Young's modulus and γ is the Poisson's ratio of the substrate, t_f and t_s are the thickness of the film and substrate, respectively, and R is the wafer curvature.

From the slope of the stress-temperature curves, the product of the biaxial modulus and the difference between the CTE of the substrate (α_s) and film (α_f) can be obtained:

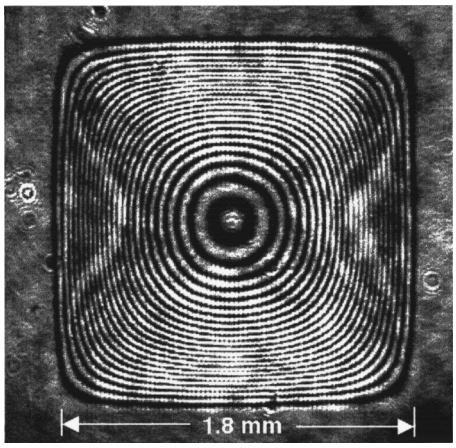

FIG. 1. Typical image of optically interfered fringes caused by a bulged dense PAE membrane.

$$d\sigma/dT = M_f(\alpha_s - \alpha_f), \tag{7}$$

where $M_f = E/(1-\gamma)$ is the biaxial modulus of a free standing film which can be determined by the membrane bulge test already discussed. Knowing M_f, α_s, and the slope, we obtain α_f.

III. RESULTS AND DISCUSSION

A. Result from the membrane bulge test

The dense PAE film sample was coated at 3000 rpm for 30 s. After curing, the surface of the dense film was smooth, and the film thickness was measured to be 460 ± 10 nm. The side of a dense PAE window is 1.60 mm. The porous PAE film was double-coated at 4000 rpm for 30 s. The surface roughness of the porous film can be measured to be in the order of 40 nm, and the total thickness was 1180 ± 20 nm. The side of a porous PAE window is 1.80 mm.

A laser interferometer was used to measure the maximum membrane deflection. A typical image of optically interfered fringes caused by a bulged dense PAE membrane is shown in Fig. 1. The raw data from a bulge test provide the deflection profile of the membrane, δ, versus the differential pressure P. The curve of maximum δ vs P is shown in Fig. 2(a). Although the P vs δ curve is almost linear in this pressure range, we found that the effect of the initial stress dominates that of membrane deformation in this pressure range. Therefore, the results are very unreliable because the initial stress σ_i in the film was calculated to be 35.2 ± 0.2 MPa after a curve fitting of Fig. 2(a) using Eq. (1). Instead, we used Eqs. (2) and (3) to calculate the stress σ and strain S. In the calculation, the small membrane deflection region was rejected, because in this region the deflection measurement accuracy was relatively low. The biaxial modulus of the dense PAE film was estimated to be 6.84 ± 0.77 GPa based on the curve fitting of the $\sigma - S$ curve, as shown in Fig. 2(b).

For the porous film the initial stress σ_i was calculated to be 15.8 ± 0.2 MPa and the biaxial modulus was estimated to be 3.53 ± 0.7 GPa based on the curve fitting of the $\sigma - S$ curve. Figure 3(a) shows the maximum membrane deflection δ versus the differential pressure P curve and Fig. 3(b) the stress σ versus strain S curve for the porous PAE film.

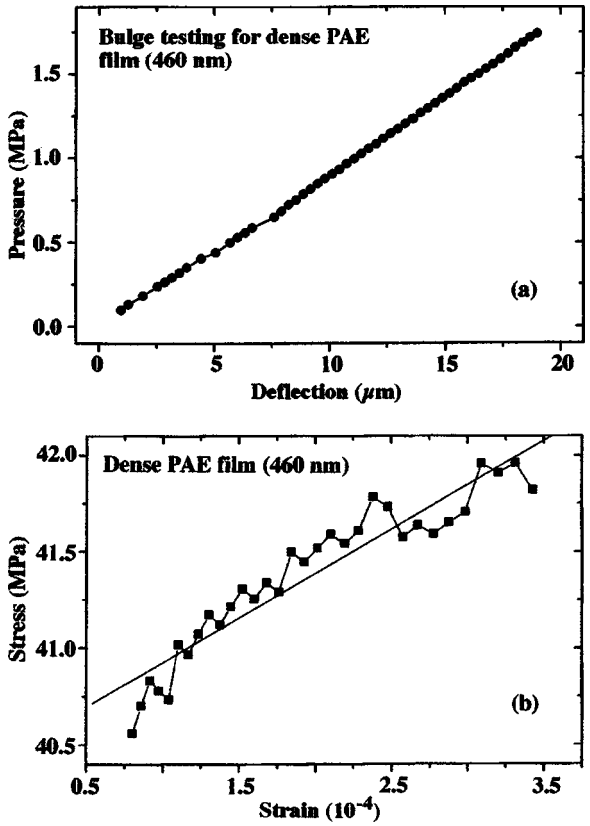

FIG. 2. Maximum membrane deflection δ vs the differential pressure P curves (a) for a dense PAE film, and the stress σ vs stain S curves (b) calculated from the data in (a).

From the data of the biaxial modulus taking the Poisson's ratio of 0.42, the elastic modulus of dense and porous PAE films can be calculated to be 3.96 ± 0.45 and 2.04 ± 0.41 GPa, respectively. Both are higher than that of the unmodified PAE which has a value of 1.8 GPa reported in Ref. 13.

B. Result from nanoindentation

The elastic modulus E and hardness H of the 1-μm-thick dense PAE film as a function of indentation depth or displacement is shown in Fig. 4. The value of E drops prominently with decreasing indentation depth. The data points acquired below depths of 30 nm ($<3\%$ of the film thickness) are averaged and give an average E of 3.91 ± 0.41 GPa. This value is very close to that obtained from the bulge test [3.96 ± 0.45 GPa, which was calculated from the biaxial modulus $E/(1-\gamma)$, taking $\gamma = 0.42$], shown in the last section. The data points of H are less dependent on indentation depth, where the averaged value below indentation depth of 30 nm is 0.32 ± 0.04 GPa.

The results of the 1-μm-thick porous PAE film sample are shown in Fig. 5. The data points show similar indentation depth dependence. The average E from the data points of indentation depths below 30 nm is exactly equal to that (3.91 GPa) of the 1-μm-thick dense film, reflecting very little effect of the pores introduced into the film. However, we recall that the value of E of the porous film measured by the bulge test is 2.04 ± 0.41 GPa, much lower than that of the average

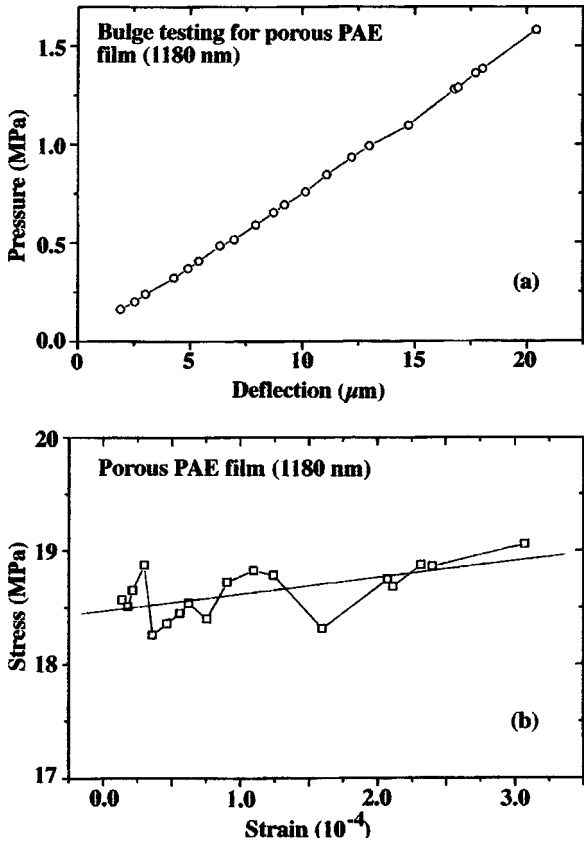

FIG. 3. Maximum membrane deflection δ vs the differential pressure P curves (a) for a porous PAE film, and the stress σ vs stain S curves (b) calculated from the data in (a).

E obtained by nanoindentation. This discrepancy is explained if one considers that the tip size in a nanoindentation test is so small that, in most cases, it mainly touches the matrix of the film, so the matrix part dominates the result.

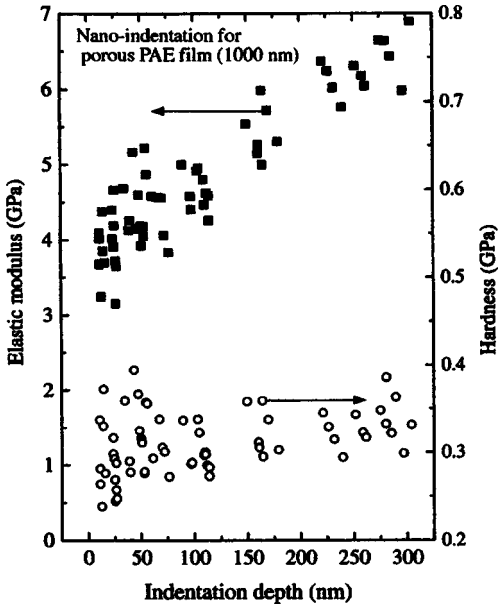

FIG. 5. Elastic modulus E and hardness H of a 1-μm-thick porous PAE film sample as functions of indentation depth.

But the presence of the pores induces a stronger scattering of the data points at small depths as indicated in Fig. 5. On the other hand, the bulge test detects the macroscopic average of the film, and is more likely to include the effects of the pores. The hardness of the 1-μm-thick dense sample is less dependent on the indentation depth, but in the porous film the average hardness below indentation depth of 30 nm is 0.29 ± 0.04, which is 9% lower that that of the 1-μm-thick dense film, partly reflecting the influences of the pores.

The results of a thin (300 nm) dense film are shown in Fig. 6. The data points of E show much stronger indentation depth dependence. The average E calculated from the data

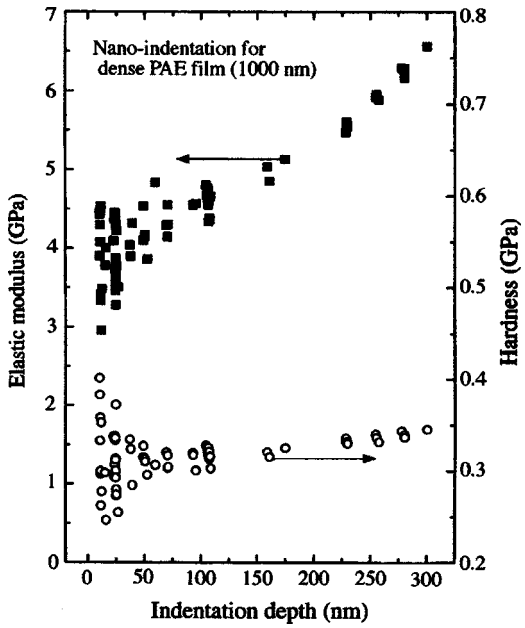

FIG. 4. Elastic modulus E and hardness H of a 1-μm-thick dense PAE film sample as functions of indentation depth.

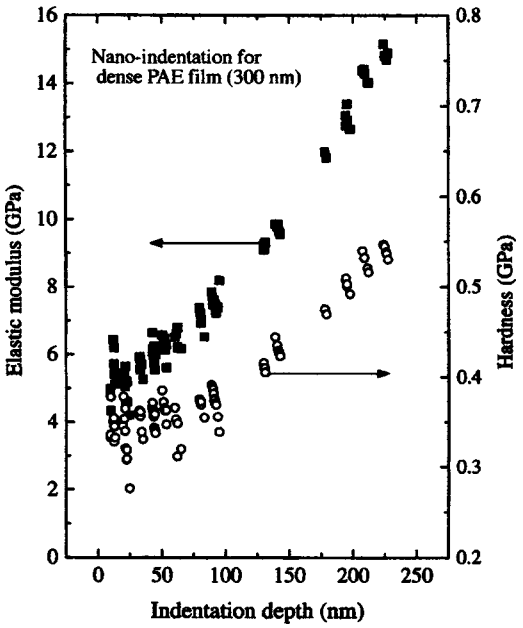

FIG. 6. Elastic modulus E and hardness H of a thin (300 nm) dense PAE film sample as functions of indentation depth.

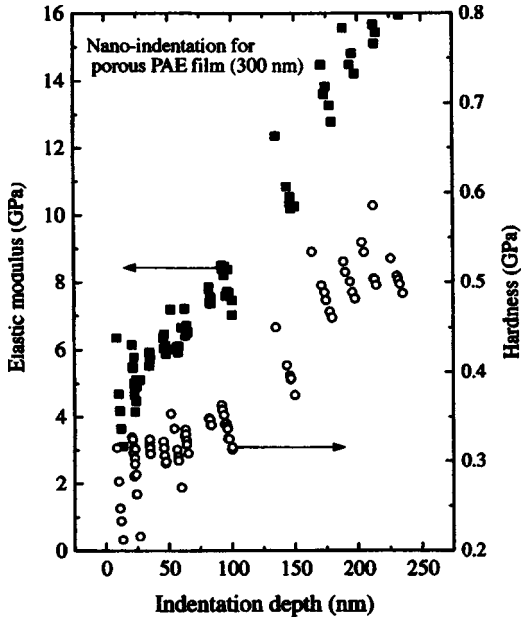

FIG. 7. Elastic modulus E and hardness H of a thin (300 nm) porous PAE film sample as functions of indentation depth.

points at indentation depths smaller than 30 nm (10% of the film thickness) is 5.19 ± 0.58 GPa, namely 1.3 times of that obtained using bulge test. This result is attributed to the stronger substrate effect for a soft film on a hard substrate when the film thickness decreases, and is generally observed in polymer-on-silicon systems. For example, Lucas *et al.*[28] reported that the substrate effect for indentation test of polymer film starts to be observable at indentation depths of 5%–10% of the film thickness. This is why the results of the nanoindentation and bulge test match quite well for the thick dense sample when the indentation depths are lower than 3% of the film thickness. The average hardness H (at indentation depth smaller than 30 nm) for this dense film is 0.34 ± 0.03 GPa.

Figure 7 shows that the results E and H of a thin (300 nm) porous film sample, for which the average value of E and H at indentation depths smaller than 30 nm are 4.88 ± 0.8 and 0.28 ± 0.03 GPa, respectively. They are 6% and 18%, respectively, lower than the corresponding results of the thin (300 nm) dense sample. The decreases are quite significant. This may arise because the pores in the thin porous sample are small and they interact more strongly with the indenter tip during indentation, hence the effects of the pores are more important. Different film thickness may affect the measured value of E, but likely has no effect on H. Table I lists E and H for porous PAE samples with different film thickness. Figure 8 shows the dependence of elastic modulus E and hardness H on the thickness of porous PAE film samples.

TABLE I. Variation of E and H with film thickness of porous PAE samples (by nanoindentation measurement).

Film thickness t (nm)	Elastic modulus E (GPa)	Hardness H (GPa)
300 ± 10	4.88 ± 0.84	0.28 ± 0.03
485 ± 10	4.55 ± 0.41	0.29 ± 0.03
800 ± 20	4.27 ± 0.52	0.27 ± 0.03
1000 ± 20	3.91 ± 0.41	0.29 ± 0.04

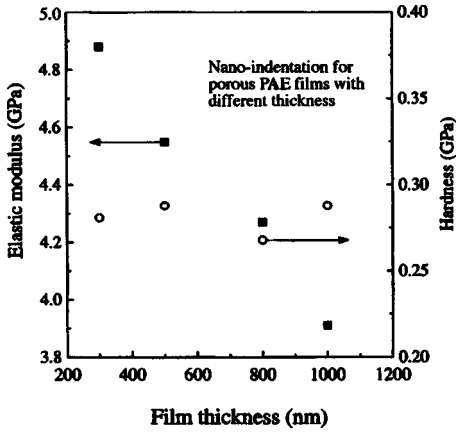

FIG. 8. Elastic modulus E and hardness H of porous PAE film samples with different thickness.

C. CTE and initial stress

Figures 9(a) and 9(b) show the stress-temperature curves of the dense ($t = 760$ nm) and porous ($t = 1000$ nm) PAE films, respectively, measured by the single-substrate bending beam method. The slopes of the curves are negative and nearly linear. The temperature was ramped up linearly from room temperature (25 °C) to 400 °C for the dense film (or 380 °C for porous film) in 1.75 h, held at 400 °C (or 380 °C)

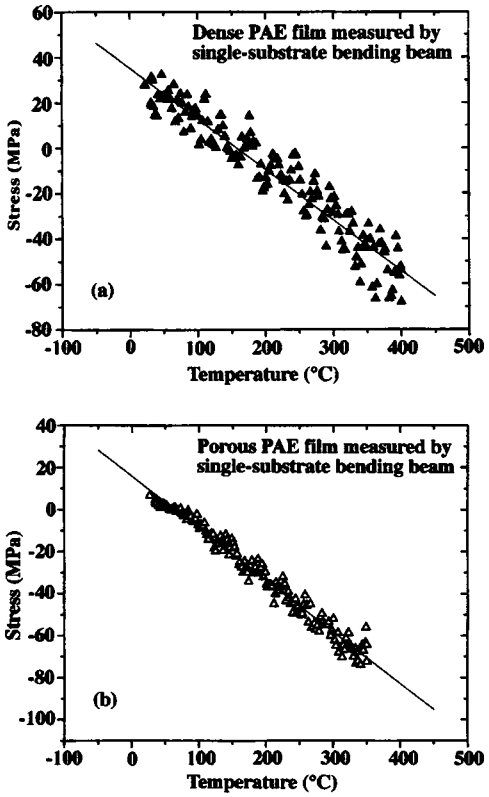

FIG. 9. Stress-temperature curves of a dense ($t = 760$ nm) PAE films (a) and a porous ($t = 1000$ nm) PAE films (b).

TABLE II. Mechanical properties of dense and porous PAE films obtained from different methods.

Method	Property	Result of dense film	Result of porous film
See Ref. 15	Dielectric constant ε'	2.71 ± 0.05	1.83 ± 0.05
See Ref. 15	Porosity (estimated) (%)	0	40 ± 4
Membrane bulge test	Biaxial modulus $E/(1-\gamma)$ (GPa)	6.84 ± 0.77	3.53 ± 0.7
	Elastic modulus E (GPa), $\gamma=0.42$	3.96 ± 0.45	2.04 ± 0.41
	Initial stress σ_i (MPa)	35.2 ± 0.2	15.8 ± 0.2
Nanoindentation	Elastic modulus E (GPa), 1 μm film	3.91 ± 0.41	3.91 ± 0.41
	Hardness H (GPa)	0.32 ± 0.04	0.29 ± 0.04
Single-substrate bending beam method	Initial stress σ_i (MPa)	32 ± 3	16 ± 2
	CTE α_f (ppm/°C)	26.8–32.6 (25–350 °C)	56.1–72.5 (25–350 °C)

for 0.25 h, and then decreased down to room temperature in 2 h. Four samples of each kind were tested. It was found that the initial stress and the slope of the stress-temperature curve varied significantly from sample to sample. The initial stress σ_i of the dense and porous film varied from 32 to 68 MPa and 16 to 78 MPa, respectively. However, there are two samples (one dense and one porous) having the initial stresses which are in excellent agreement with the results from the bulge test measurement (35.2 ± 0.2 MPa for the dense film, and 15.8 ± 0.2 MPa for the porous film). The discrepancy for the other samples tested by the single-substrate bending beam method is tentatively attributed to the difference in the solution and the cooling temperature profile during curing. In general, the initial stress measured by the bulge test is lower than that by the single-substrate bending beam method. This may be due to stress relaxation in the film after part of the substrate silicon was removed in the bulge test. During the cycling process, both dense and porous films are in the tensile stress region. No cracking can be seen under an optical microscope after several repeated cycles. In Fig. 9, the slope for the dense film ranges from 1.526 to 1.923×10^5 Pa/°C, and the porous film from 1.889 to 2.466 $\times10^5$ Pa/°C. The higher the temperature, the greater the slope. Taking the biaxial modulus M_f measured by the bulge test and the CTE of silicon substrate to be 2.8 ppm/°C, the calculated CTE of the films range from 26.8 to 32.6 ppm/°C (25–350 °C) for the dense PAE film and 56.1 to 72.5 ppm/°C (25–350 °C) for porous PAE film. The data of CTE for the dense modified PAE is smaller by 50% than that for the unmodified PAE reported in Ref. 13. In addition, the CTE of porous PAE films is larger than that of dense PAE films due to the presence of the pores. The pores contain air but not other gas, that has been identified by FTIR spectra. Based on ideal gas law, CTE of ideal gas equals to $(273.16\,\mathrm{K})^{-1}$ or $3.66\times10^{-3}(°\mathrm{C})^{-1}$, which is much higher than that of the dense PAE. Therefore, the CTE of porous PAE, as a two-phase material, should be bigger than that of dense PAE. Table II summarizes the data obtained by the above three techniques.

D. Poisson's ratio

In the above measurements and calculations, Poisson's ratio γ of 0.42 was used. We attempted to use different values of Poisson's ratio from 0.40 to 0.43 for calculating the elastic modulus from the measured biaxial modulus. We found that when $\gamma=0.42$ was used and we obtained, the best match between the initial stress measured by the bulge test and that calculated from the stress versus temperature curve by the single-substrate bending beam method. Also, the elastic modulus calculated from the bulge test is in good agreement with that measured by nanoindentation.

IV. CONCLUSIONS

(1) Mechanical properties and coefficient of thermal expansion of low-ε' dense PAE and porous PAE film samples were measured by three different methods; membrane bulge test, nanoindentation, and single-substrate bending beam method. For the dense film samples, a Young's modulus of 3.9 GPa was obtained independently from both the bulge test and nanoindentation methods. The initial stress of 35 and 16 MPa for the dense and porous film samples, respectively, were also obtained from both the bulge test and single-substrate bending beam methods. Hardness of 0.32 and 0.29 GPa for the dense and porous 1-μm-thick films, respectively, were obtained from nanoindentation. CTE of 26.8–32.6 ppm/°C and 56.1–72.5 ppm/°C for dense and porous PAE films, respectively, were obtained by single-substrate bending beam method.

(2) The elastic modulus obtained from nanoindentation depends significantly on the film thickness as well as the displacement depth of the indenter. The substrate effect was observed. We measured E and H of dense and porous PAE films with a thickness of 1 μm at indentation depths as small as 10 nm ($\sim$1% film thickness), to see how it is affected by the substrate. We found that when the indentation depths are below 30 nm for a 1-μm-thick film (displacement $<$3% of the film thickness), the average of E agrees with that obtained from the bulge test but H does not depend on thickness, rather it depends on the indentation depth for thinner (300 nm) films.

(3) The Poisson's ratio of 0.42 for PAE films was estimated by iteration of calculation. Using this value, we found that the elastic modulus as well as the initial stress are in good agreement among the results deduced from the different methods used.

(4) For the porous PAE films the discrepancy between elastic modulus data obtained from the bulge test and nanoindentation can be explained as below. Because the tip size in a nanoindentation test is so small that, in most cases, it mainly touches the matrix of the film, the matrix part dominates the result. On the other hand, the bulge test detects the macroscopic average of the film, so the resulting modulus includes the effect of pores.

ACKNOWLEDGMENTS

This work was partly supported by UC-SMART Project No. SM98-08. The authors would like to thank Professor Yang Yang and Tung-Fung Guo (UCLA) for their help in using the FTIR facility.

[1] The National Technology Roadmap for Semiconductors, Semiconductor Industry Association, San Jose, CA (1997).
[2] W. W. Lee and P. S. Ho, MRS Bull. **22**, 19 (1997).
[3] J. P. Sullivan, D. R. Denison, J. C. Barbour, P. P. Newcomer, C. A. Apblett, C. H. Seager, and A. G. Baca, Mater. Res. Soc. Symp. Proc. **443**, 149 (1997).
[4] K. Endo, MRS Bull. **22**, 55 (1997).
[5] R. S. List, A. Singh, A. Ralston, and G. Dixit, MRS Bull. **22**, 61 (1997).
[6] N. H. Hendricks, Mater. Res. Soc. Symp. Proc. **443**, 3 (1997).
[7] R. N. Vrtis, K. A. Heap, W. F. Burgoyne, and L. M. Robeson, Mater. Res. Soc. Symp. Proc. **443**, 171 (1997).
[8] R. D. Miller, J. L. Hedrick, D. Y. Yoon, R. F. Cook, and J. P. Hummel, MRS Bull. **22**, 44 (1997).
[9] A. T. Kohl, R. Mimna, R. Shick, L. Rhodes, Z. L. Wang, and P. A. Kohl, Electrochem. Solid-State Lett. **2**, 77 (1999).
[10] C. M. Jin, J. D. Luttmer, D. M. Smith, and T. A. Ramos, MRS Bull. **22**, 39 (1997).
[11] C. H. Ting and T. E. Seidel, Mater. Res. Soc. Symp. Proc. **381**, 3 (1995).
[12] B. Zhao, S.-Q. Wang, M. Fiebig, S. Anderson, P. K. Vasudev, and T. E. Seidel, IEEE International Reliability Physics Proceedings (1996) pp. 156–163.
[13] E. T. Ryan, A. J. McKerrow, J. Leu, and P. S. Ho, MRS Bull. **22**, 49 (1997).
[14] L. Peters, Semiconductor **21**, 64 (1998).
[15] Y. Xu, Y. Tsai, K. N. Tu, B. Zhao, Q. Z. Liu, M. Brongo, G. T. T. Sheng, and C. H. Tung, Appl. Phys. Lett. **75**, 853 (1999).
[16] C. N. Liao, Y. P. Tsai, Y. Xu, K. N. Tu, B. Zhao, Q. Z. Liu, and M. Brongo, J. Appl. Phys. (submitted).
[17] W. W. Lee and P. S. Ho, MRS Bull. **22**, 19 (1997).
[18] M. Morgen, E. T. Ryan, J.-H. Zhao, C. Hu, T. Cho, and P. S. Ho, J. Met. 37 (1999).
[19] J. W. Beams, in *Structure and Properties of Thin Films*, edited by C. A. Neugebauer, J. B. Newkirk, and D. A. Vermilyea (Wiley, New York, 1959), p. 183.
[20] D. Maier-Schneider, A. Ersoy, J. Maibach, D. Schneider, and E. Obermeier, Sens. Mater. **7**, 121 (1995).
[21] J. Y. Pan, P. Lin, F. Maseeh, and S. D. Senturia, in *Technical Digest IEEE Solid-State Sensors and Actuators Workshop* (IEEE, New York, 1990), p. 70.
[22] M. G. Allen, M. Mehregany, R. T. Howe, and S. D. Senturia, Appl. Phys. Lett. **51**, 241 (1987).
[23] W. R. LaFontaine, C. A. Paszkiet, M. A. Korhonen, and C. Y. Li, J. Mater. Res. **6**, 2084 (1991).
[24] G. M. Pharr and W. C. Oliver, MRS Bull. **17**, 28 (1992).
[25] D. W. Zheng, Y. Xu, Y. P. Tsai, K. N. Tu, P. Patterson, B. Zhao, Q. Z. Liu, and M. Brongo, Appl. Phys. Lett. **75**, 2008 (2000).
[26] D. W. Zheng, Ph.D dissertation, University of California at Los Angeles, 1999.
[27] W. C. Oliver and G. M. Pharr, J. Mater. Res. **7**, 1564 (1992).
[28] B. N. Lucas, C. T. Rosenmayer, and W. C. Oliver, Mater. Res. Soc. Symp. Proc. **505**, 97 (1998).